Biochemical and Biophysical Research Communications 427 (2012) 466–472

Contents lists available at SciVerse ScienceDirect

Biochemical and Biophysical Research Communications

journal homepage: www.elsevier.com/locate/ybbrc

$GABA_A$ receptor-mediated feedforward and feedback inhibition differentially modulate hippocampal spike timing-dependent plasticity

Hyun Jae Jang, Jeehyun Kwag *

Department of Brain and Cognitive Engineering, Korea University, Seoul, Republic of Korea

ARTICLE INFO

Article history:
Received 1 August 2012
Available online 24 August 2012

Keywords:
Hippocampus
Spike timing-dependent plasticity
Interneuron
Feedback inhibition
Feedforward inhibition
NEURON simulation model

ABSTRACT

Synaptic plasticity is believed to play an important role in hippocampal learning and memory. The precise and relative timing of pre- and postsynaptic activity has been shown to determine the sign and amplitude of hippocampal synaptic plasticity through spike timing-dependent plasticity (STDP). While most studies on STDP have mainly focused on excitatory synapses, neural networks are composed not only of excitatory synapses, but also of inhibitory synapses. Interneurons are known to make inhibitory synaptic connections with hippocampal CA1 pyramidal neurons through feedforward and feedback inhibitory networks. However, the roles of different inhibitory network structures on STDP remain unknown. Using a simplified hippocampal network model with a deterministic Ca^{2+} dynamics-dependent STDP model, we show that feedforward and feedback inhibitory networks differentially modulate STDP. Moreover, inhibitory synaptic weight and synaptic location influenced the STDP profile. Taken together, our results provide a computational role of inhibitory network in STDP and in memory processing of hippocampal circuits.

1. Introduction

Synaptic plasticity is believed to serve an important role in hippocampal memory function [1]. The precise and relative timing of pre- and postsynaptic spikes has been shown to determine the amplitude and the sign of plasticity through spike timing-dependent plasticity (STDP) [2,3]. A single presynaptic spike preceding a single postsynaptic spike with a time window (Δt) of ~20 ms induces timing-dependent long-term potentiation (tLTP), while the reversed pairing order induces timing-dependent long-term depression (tLTD) at hippocampal excitatory synapses in culture [2]. However, hippocampal networks are not simply composed of excitatory neurons alone, but they also consist of a diverse variety of interneurons (IN) [4]. Single-spike pairing-induced tLTP is readily observed in juvenile hippocampal CA3–CA1 synapses [5,6], but it is blocked with the developmental maturation of $GABA_A$ receptor-mediated inhibitory networks [6,7]. Inhibition is believed to block the back-propagating action potentials (bAP) [8] that are required for the activation of NMDA receptors. Thus, it seems that $GABA_A$ receptor-mediated inhibition is involved in shaping STDP profiles, as reported in *in vitro* [6,9] and *in silico* experiments [10,11]. However, the roles of different types of INs on STDP remain unknown.

$GABA_A$ receptor-mediated inhibition can be provided by different types of INs [4]. One way to classify them is to group them into feedforward or feedback inhibitory networks [12–15], according to their synaptic networks to pyramidal cells (PCs). In feedforward inhibition, INs receive afferent excitatory inputs that in turn inhibit local PCs [13]. Such feedforward inhibition provides inputs that temporally overlap with afferent excitatory inputs [16], which greatly reduces the spike jitter of PCs and consequently increases the temporal fidelity [14]. In contrast, feedback inhibition is recruited by the recurrent activation of PCs [12,13] and this can limit the spread of excitation in local PC populations [17]. Therefore, different inhibitory network structures seem to exist to control hippocampal pyramidal neuronal activity, which could influence the hippocampal STDP. Thus, the aim of this study is to use a hippocampal neural network model to investigate how feedforward and feedback inhibitory network differentially control STDP in hippocampal network.

2. Materials and methods

2.1. Neuronal model

The simple hippocampal network model consisted of a CA1 PC, a CA3 PC, and an IN. The CA1 PC model consisted of a soma, an apical dendrite (length = 585 μm), and a dendritic spine. The spine was modeled to be located 100 μm away from the soma on the apical dendrite (Fig. 1A). The CA3 PC was modeled as a single-

* Corresponding author. Address: Department of Brain and Cognitive Engineering, Korea University, 145 Anam-ro, Seongbuk-gu, Seoul, Republic of Korea. Fax: +82 2 926 3268.
E-mail address: jkwag@korea.ac.kr (J. Kwag).

0006-291X/$ - see front matter © 2012 Elsevier Inc. All rights reserved.
http://dx.doi.org/10.1016/j.bbrc.2012.08.081

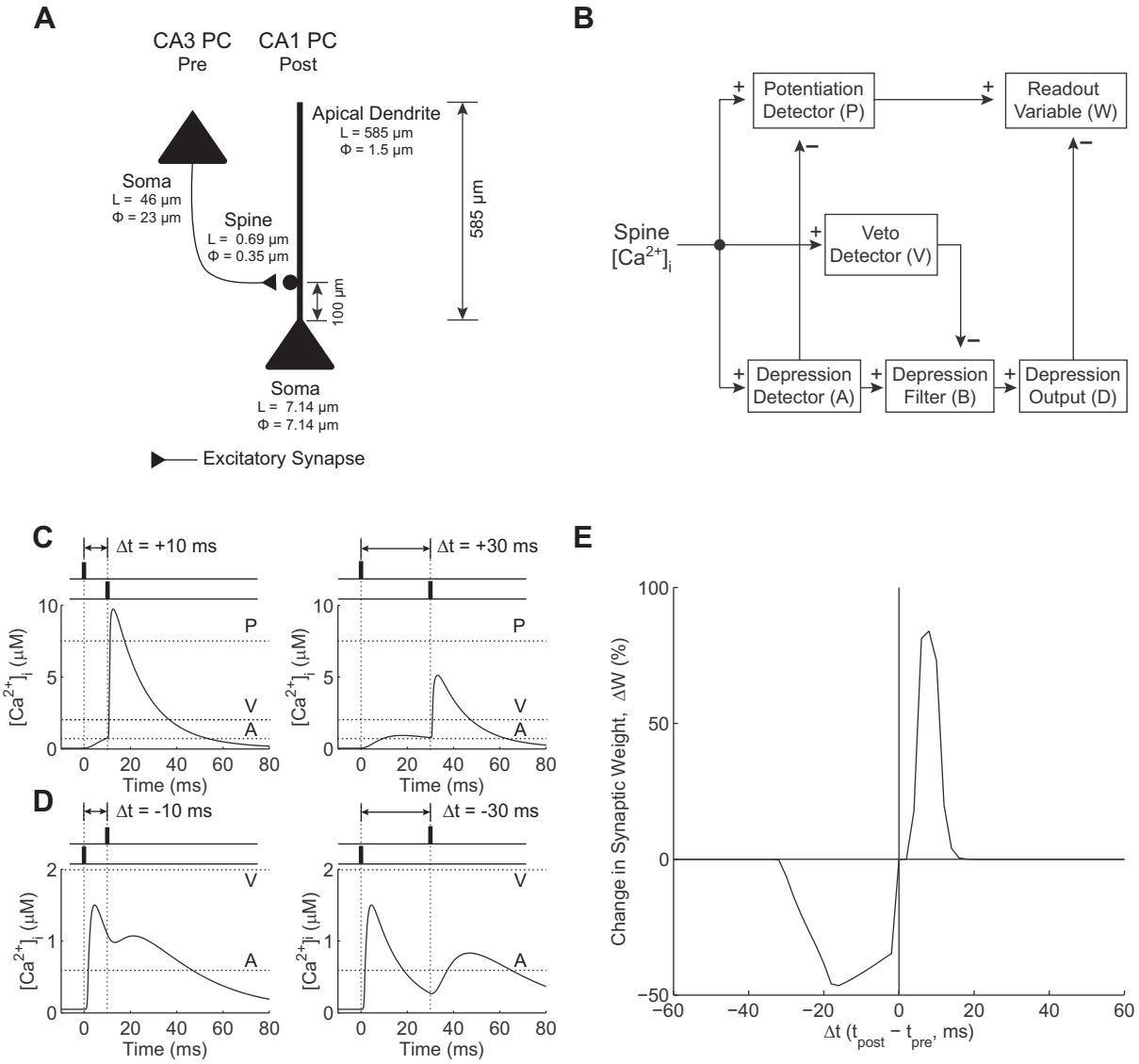

Fig. 1. Verification of the asymmetric spike timing-dependent plasticity (STDP) curve with a simple hippocampal network model. (A) A simplified hippocampal network model which includes a CA3 pyramidal cell (PC) and a CA1 PC. An excitatory CA3–CA1 synapse was modeled as a CA3 PC (pre: presynaptic neuron) synapsing onto the dendritic spine that is located 100 μm away from the soma on the apical dendrite of the CA1 PC (post: postsynaptic neuron). *L* is the length and *Φ* is the diameter of the model compartment. (B) A schematic diagram of a deterministic Ca^{2+} dynamics-dependent STDP model (modified from Rubin et al., 2005). (C and D) Single-spike pairing-induced postsynaptic spine calcium concentration ($[Ca^{2+}]_i$) plotted over time during the pre-10-post (C, left), pre-30-post (C, right), post-10-pre (D, left), and post-30-pre (D, right) pairing paradigms. (E) The change in synaptic weight (ΔW) plotted as a function of Δt, resulting in an asymmetric STDP curve.

Table 1
Passive membrane properties and voltage-gated membrane conductances of the CA1 pyramidal cell (PC), CA3 PC and Interneuron (IN) models.

Parameter	CA1 PC	CA1 PC spine	CA3 PC	IN
V_{rest} (mV)	−60	−60	−65	−65
R_m (kΩ cm^2)	28	28	20	5.6
C_m (μF/cm^2)	1	1	1	1.4
τ_m (ms)	28	28	20	7.84
R_a (Ω cm)	200	200	200	100
g_{Leak} (S/cm^2)	0.0000375	0.0000375	0.00005	0.00018
g_{Na} (S/cm^2)	0.025	0.007	0.62	0.2
g_{Kdr} (S/cm^2)	0.0031	0.000867	0.036	0.013
g_{KA} (S/cm^2)	0.042	0.012		0.00015
g_{CaL} (S/cm^2)	0.00015	0.014		
g_{AHP} (S/cm^2)	0.0005			
g_h (S/cm^2)	0.00002			
g_{KM} (S/cm^2)	0.003			

compartment spike generator [18]. The IN, which was adopted from Cutsuridis et al. [19], was reduced to a single-compartment model. All passive and active membrane properties of each component of the neuronal model are shown in Table 1. All channels were uniformly distributed apart from g_{KA} [20] and g_h [21] in the CA1 PC, whose conductance linearly increased with distance from the soma, such that

$$g_{kA}(\text{dist}) = 0.042 * (1 + \text{dist}/100)\ \text{S/cm}^2$$

$$g_h(\text{dist}) = 0.00002 * (1 + 3 * \text{dist}/100)\ \text{S/cm}^2$$

where dist (μm) is the distance from the soma.

2.2. Network connection

A CA3–CA1 synapse was modeled to be located at the dendritic spine (Fig. 1A). A single CA3 PC spike was modeled to evoke an excitatory postsynaptic potential (EPSP) at the spine of the CA1 PC through AMPA and NMDA receptors. The AMPA receptor-mediated current (I_{AMPA}) was modeled as a single-exponential

alpha function [22] in order to simulate AMPA kinetics as observed *in vitro* [23,24], such that

$$I_{\mathrm{AMPA}} = g_{\mathrm{AMPA}} * (e^{-t/\tau}) * (V_{\mathrm{m}} - E_{\mathrm{AMPA}})$$

where g_{AMPA} = 0.3 pS, τ = 7 ms, and E_{AMPA} = 0 mV.

The NMDA receptor-mediated current (I_{NMDA}) and its voltage-dependent magnesium block were modeled using the equation [22],

$$I_{\mathrm{NMDA,x}} = \frac{g_{\mathrm{NMDA,x}} * (e^{-t/\tau_{\mathrm{rise}}} - e^{-t/\tau_{\mathrm{decay}}}) * (V_m - E_{\mathrm{NMDA,x}})}{1 + ([mg]/n) * e^{-r_{\mathrm{syn}} * V_m}}, \quad x \epsilon \{\mathrm{syn}, \mathrm{ca}\}$$

where $g_{\mathrm{NMDA,syn}}$ = 1 nS, $E_{\mathrm{NMDA,syn}}$ = 0 mV, r_{syn} = 0.062, $g_{\mathrm{NMDA,Ca}}$ = 54 pS, $E_{\mathrm{NMDA,Ca}}$ = 120 mV, r_{Ca} = 0.124, τ_{rise} = 4 ms, τ_{decay} = 21 ms, n = 3.57, and magnesium concentration [mg] = 0.5 mM. *syn* stands for synaptic current, and *Ca* stands for calcium current. $g_{\mathrm{NMDA}}$was adjusted in order to satisfy the AMPA/NMDA ratio of EPSPs recorded at the CA3–CA1 synapses *in vitro* [23,25]. The concentration of the calcium influx through the spike was also modeled to reflect that recorded at the dendritic spine of CA1 PC [26].

Excitatory and inhibitory synapses were all modeled using alpha function of double exponential form, such that

$$I_{\mathrm{syn}} = g_{syn} * \mathrm{factor} * (e^{-t/\tau_{\mathrm{rise}}} - e^{-t/\tau_{\mathrm{decay}}}) * (V_m - E_{\mathrm{syn}})$$

where

$$\mathrm{factor} = \frac{1}{(-e^{-t_p/\tau_{\mathrm{rise}}} + e^{-t_p/\tau_{\mathrm{decay}}})}$$

$$t_p = \left(\frac{\tau_{\mathrm{rise}} * \tau_{\mathrm{decay}}}{\tau_{\mathrm{decay}} - \tau_{\mathrm{rise}}}\right) * log(\tau_{\mathrm{rise}}/\tau_{\mathrm{decay}})$$

Inhibition was modeled as $GABA_A$ receptor-mediated inhibition. For the inhibitory synapse between the IN and the CA1 PC (IN-CA1 synapse), g_{syn} = 10 nS, τ_{rise} = 4 ms, τ_{decay} = 15 ms, and E_{syn} = −70 mV [27,28]. For the excitatory synapse between the CA3 PC and the IN (CA3-IN synapse), g_{syn} = 30 nS, τ_{rise} = 0.05 ms, τ_{decay} = 1 ms, and E_{syn} = 0 mV [29,30]. For the excitatory synapse between the CA1 PC and the IN (CA1-IN synapse), g_{syn} = 10 nS, τ_{rise} = 0.01 ms, τ_{decay} = 0.5 ms, and E_{syn} = 0 mV [31,32].

2.3. STDP model

A deterministic Ca^{2+}-dependent STDP model was adopted from Rubin et al. (2005) [33] to simulate the STDP learning rule at the CA3–CA1 synapse (Fig. 1B). In brief, the phosphorylation cascade of Ca^{2+}/calmodulin-dependent protein kinase II was modeled as a potentiation detector (P) that was activated at intracellular Ca^{2+} concentrations ($[Ca^{2+}]_i$) over 7.5 μM (*pHC*), which triggered tLTP.

Table 2
Parameters used in the deterministic Ca^{2+}-dependent STDP model.

Parameter	Value	Parameter	Value
pHC	7.5 μM	pHN	8
aHC	2 μM	aHN	3
θ_v	0.6 μM	σ_v	−0.05
θ_d	2.5	σ_d	−0.01
θ_b	0.55	σ_b	−0.02
τ_p	500 ms	k_p	−0.015
τ_a	5 ms	k_d	−0.0015
τ_v	10 ms	α_v	1.0
τ_d	250 ms	α_d	1.0
τ_b	40 ms	α_b	5.0
c_p	5	c_d	4
τ_w	500 ms	p	0.2
α_w	0.8	d	0.01
β_w	0.6		

The kinetics of dephosphorylation agents, such as protein phosphatase 1, were modeled as depression detectors (A) that were activated at $[Ca^{2+}]_i$ above 0.6 μM (*aHC*), which triggered tLTD. The competition between kinases and phosphatases, was modeled as a veto detector (V) that was activated above 2 μM (θ_v), which suppresses the induction of tLTD. Two depression agents, a depression filter (B) and a depression output (D), also controlled the induction of tLTD. All of these detectors responded to the instantaneous level and time course of $[Ca^{2+}]_i$ according to the following equations and the corresponding parameters are presented in Table 2. The interactions of each components of the STDP model gave rise to synaptic weights with the readout variable, W (Fig. 1B).

$$P' = p_\sigma([Ca^{2+}]_i) - c_p \mathrm{AP}/\tau_p$$

$$V' = v_\sigma([Ca^{2+}]_i) - V/\tau_v$$

$$A' = a_\sigma([Ca^{2+}]_i) - A/\tau_a$$

$$B' = b_\sigma(A) - B - c_d BV/\tau_b$$

$$D' = d_\sigma(B) - D/\tau_d$$

$$W' = \left(\alpha_w/\left(1 + e^{((P-p)/k_p)}\right) - \beta_w/\left(1 + e^{((D-d)/k_d)}\right) - W\right)/\tau_w$$

where

$$P_\sigma(x) = \frac{10(x/pHC)^{pHN}}{1 + (x/pHC)^{pHN}}$$

$$a_\sigma(x) = \frac{10(x/aHC)^{aHN}}{1 + (x/aHC)^{aHN}}$$

$$f_\sigma(x) = \frac{\alpha_f}{1.0 + e^{((x-\theta_f)/\sigma_f)}}, \text{for} \quad f \in \{v, d, b\}$$

2.4. Simulation environment

STDP was induced at the CA3–CA1 synapse by pairing single pre- and postsynaptic spikes with a time window (Δt) (Figs. 1–3) that was repeated 30 times at 1 Hz. A brief step-pulse was used to evoke a single spike at the CA1 and CA3 PC (2-ms duration, 0.6 nA). Δt between the pre- and postsynaptic spikes was varied in 2-ms time-steps (Figs. 1C–D, 2C–F, and 3C–F), and the STDP curve (Figs. 1E, 2G–H, and 3G–H) was plotted by calculating the change in synaptic weight (ΔW) as a function of Δt. All simulations were performed with the NEURON program [18] using a sampling rate of 10 kHz.

3. Results

3.1. Verification of the asymmetric STDP with a simple CA3–CA1 neuron network model

We first set out to verify that our simple neuron network model could reliably simulate the classical STDP curve [2]. Pairing a single presynaptic CA3 PC spike before a single postsynaptic CA1 spike with Δt = +10 ms (pre-10-post) resulted in a sharp rise of dendritic spine $[Ca^{2+}]_i$ above the tLTP detector (P) threshold of 7.5 μM (Fig. 1C, left). However, the same pairing order, but with Δt = +30 ms (pre-30-post), reduced the spine $[Ca^{2+}]_i$ below the P threshold (Fig. 1C, right). When the pairing order was reversed with Δt = −10 ms (post-10-pre), such a pairing resulted in spine $[Ca^{2+}]_i$ with 2 peaks below the veto detector (V) threshold (2 μM) near the tLTD detector (A) value (0.6 μM, Fig. 1D, left). With a post-30-pre pairing, the spine $[Ca^{2+}]_i$ of the second peak was even

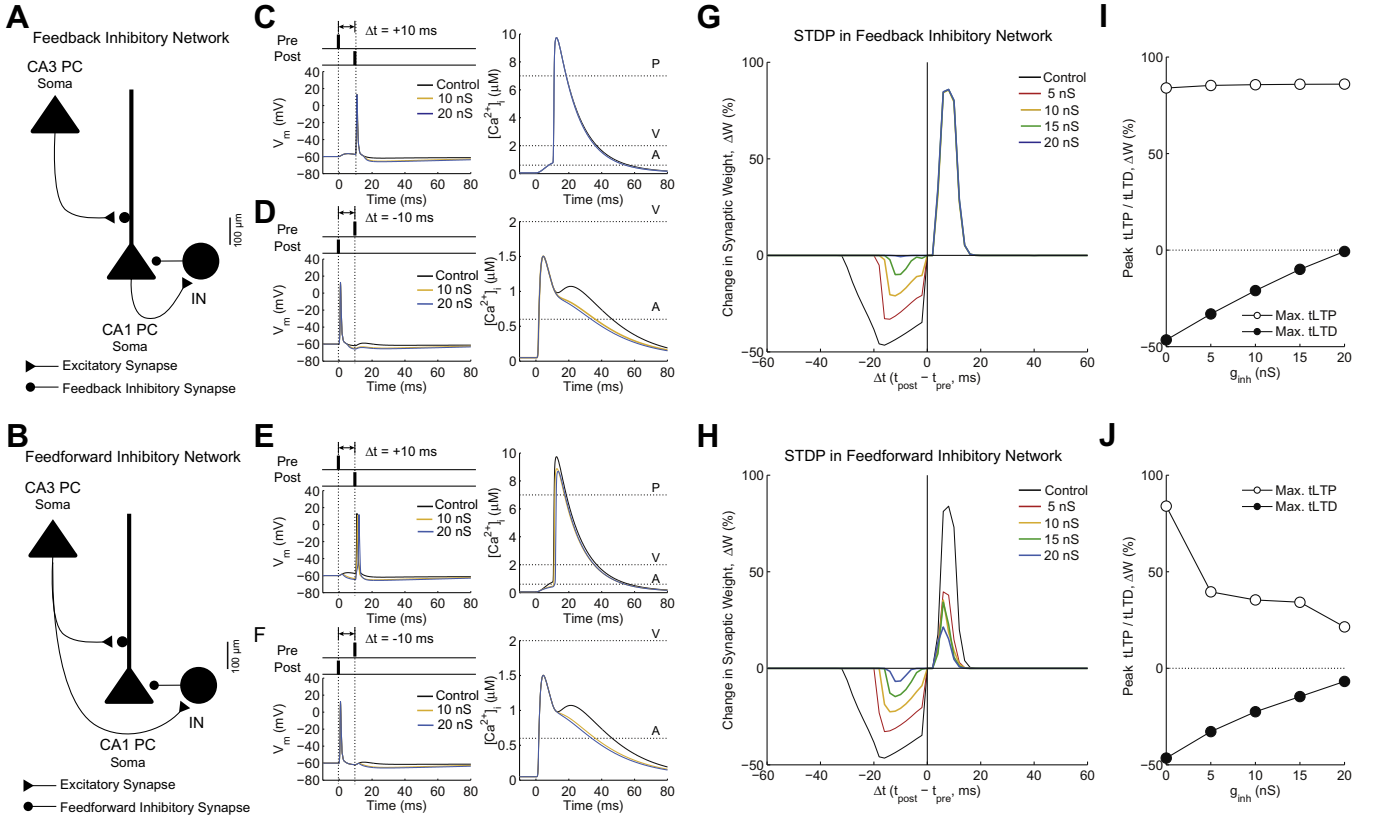

Fig. 2. Differential modulation of STDP by feedforward and feedback inhibition network. (A and B) A schematic diagram of the feedback inhibitory hippocampal network model. An excitatory CA3–CA1 synapse was modeled as a CA3 PC synapsing onto the dendritic spine that is located 100 μm away from the soma on the apical dendrite of a CA1 PC. In feedback inhibition, an interneuron (IN) receives an excitatory input from the CA1 PC, and it sends inhibitory input back to the CA1 PC. In feedforward inhibition, an IN receives an excitatory input from a CA3 PC, and it sends inhibitory input to the CA1 PC (B). (C and D) The pre- and postsynaptic spike pairing paradigm (left top), membrane voltage trace of the CA1 PC (left bottom), and the spine calcium concentrations ($[Ca^{2+}]_i$, right) during the pre-10-post (C) and the post-10-pre (D) pairing paradigms in the absence (control: black trace) and in the presence of feedback inhibition with g_{inh} = 10 and 20 nS (yellow and blue traces, respectively). (E and F) Same plots as C and D but with feedforward inhibition. (G and H) ΔW plotted as a function of Δt while varying the maximal g_{inh} between 0 and 20 nS of feedback (G) and feedforward (H) inhibition network. (I and J) The peak ΔW of tLTP (empty circle) and tLTD (filled circle) plotted as a function of feedback g_{inh} (I) and feedforward g_{inh} (J).

more reduced (Fig. 1D, right). Plotting ΔW as a function of Δt resulted in the classical asymmetric STDP curve (Fig. 1E) as observed at the hippocampal excitatory synapses of cultured hippocampal neurons [2].

3.2. Differential modulation of STDP by feedforward and feedback inhibition networks

After confirming that our model could simulate the classical asymmetric STDP curve at the CA3–CA1 synapse (Fig. 1E), we next investigated the effect of $GABA_A$ receptor-mediated inhibitory network structure on the STDP curve (Fig. 2A–B). In the presence of feedback inhibition to the somatic region of the CA1 PC (Fig. 2A), the CA1 PC spike activated the IN during the pre-10-post and the post-10-pre pairings (Fig. 2C left, 2D left). The spine $[Ca^{2+}]_i$ during the pre-10-post pairing in the presence of feedback inhibition conductance (g_{inh}) of 10 nS (Fig. 2C right, yellow trace) was comparable to that in the control condition without feedback inhibition (Fig. 2C right, black trace). Increasing the feedback g_{inh} to 20 nS did not influence the spine $[Ca^{2+}]_i$ either (Fig. 2C right, blue trace). However, the spine $[Ca^{2+}]_i$ during the post-10-pre pairing in the feedback inhibitory network decreased with increasing g_{inh} (Fig. 2D right, blue trace). Subsequent plotting of the STDP curve revealed that the feedback inhibitory network modulated only the tLTD by suppressing it (Fig. 2G). The suppression of tLTD was g_{inh} amplitude-dependent (Fig. 2I, filled circles) while tLTP was g_{inh} amplitude-independent (Fig. 2I, empty circles).

When the simulation was repeated in the presence of feedforward inhibition to the somatic region of the CA1 PC (Fig. 2B), the CA3 PC spike activated the IN during the pre-10-post and the post-10-pre pairings (Fig. 2E left, 2F left). The spine $[Ca^{2+}]_i$ during both the pre-10-post and the post-10-pre pairings in the presence of feedforward g_{inh} = 10 nS decreased (Fig. 2E right, F right, yellow trace) compared to that in the control condition without feedforward inhibition (Fig. 2E–F, black trace). Increasing the feedforward g_{inh} amplitude to 20 nS suppressed the spine $[Ca^{2+}]_i$ even more (Fig. 2E right, 2F right, blue trace). The resulting STDP curve showed suppression of both tLTP and tLTD (Fig. 2H). When the peak ΔW of the STDP curve was plotted as a function of g_{inh} amplitude, we found that the suppression of both tLTP and tLTD was g_{inh} amplitude-dependent (Fig. 2J). These results suggest that tLTP and tLTD are differentially modulated by feedforward and feedback inhibition at the CA3–CA1 network.

3.3. Feedforward and feedback inhibitory synapse location-dependent modulation of STDP

The INs in our simple feedforward and feedback inhibitory network models were modeled to synapse onto the CA1 PC soma (Fig. 2A–B). However, there exists a diverse variety of hippocampal INs that target different dendritic domains of CA1 PCs [4,34–36]. Therefore, in order to incorporate the diversity of IN synapse locations, we repeated the simulation and varied the feedforward and feedback inhibitory synapse locations while keeping

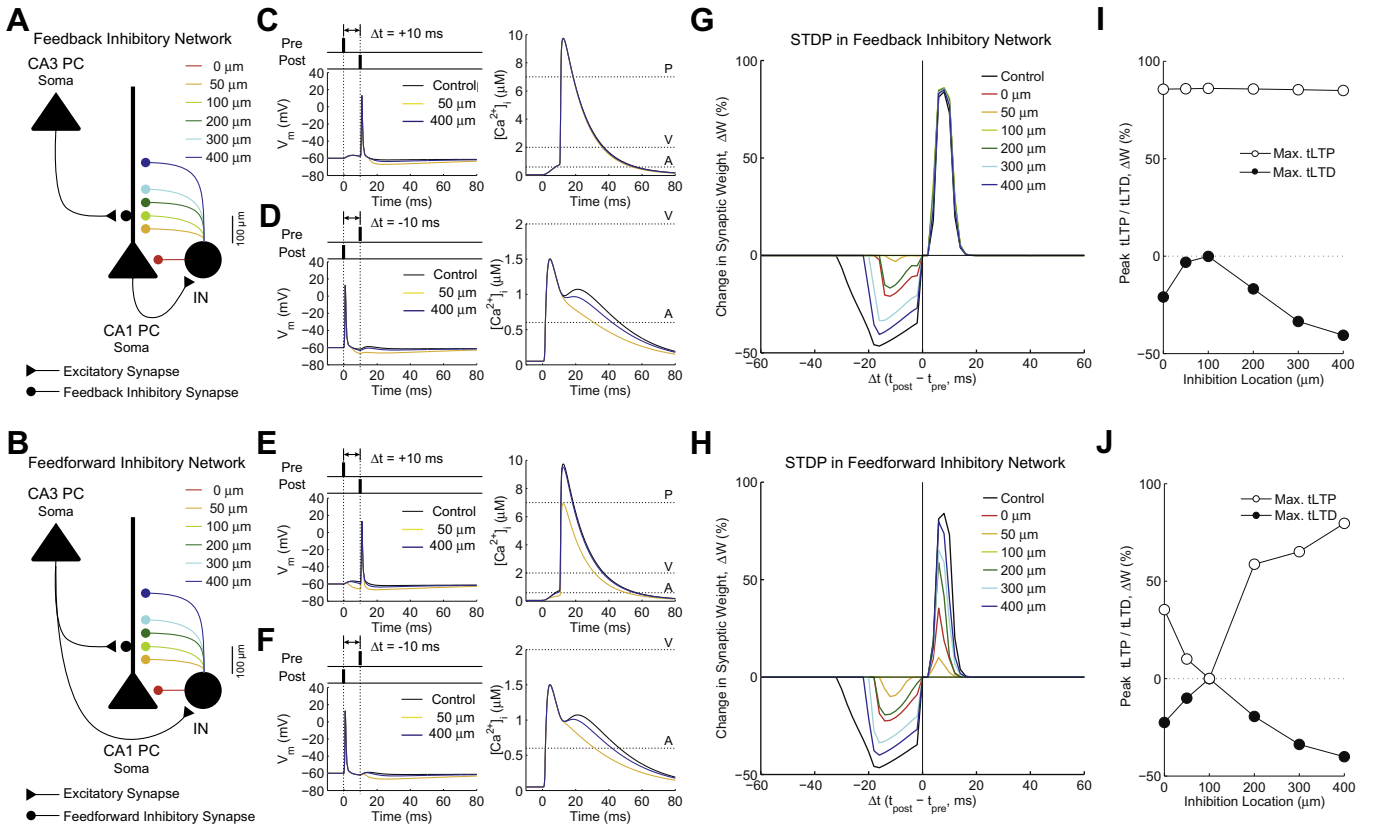

Fig. 3. Feedforward and feedback inhibitory synapse location-dependent modulation of STDP. (A and B) A schematic diagram of a feedback (A) and feedforward (B) inhibitory hippocampal network model with inhibitory synaptic locations at 0–400 μm with g_{inh} = 10 nS. (C and D) The pre- and postsynaptic neuron pairing paradigm (left top), membrane voltage trace of the CA1 PC (left middle), and the spine calcium concentration ($[Ca^{2+}]_i$, right) during the pre-10-post (C) and the post-10-pre pairing paradigms (D) in the absence (control: black trace) and presence of a feedback inhibitory input at 50 and 400 μm (yellow and blue traces, respectively). (E and F) Same plots as C and D but with feedforward inhibition. (G and H) ΔW plotted as a function of Δt while varying the inhibitory synapse locations between 0–400 μm of feedback (G) and feedforward inhibition network (H). (I and J) The peak ΔW of tLTP (empty circle) and tLTD (filled circle) plotted as a function of feedback g_{inh} (I) and feedforward g_{inh} (J).

g_{inh} = 10 nS. In the presence of a feedback inhibitory synapse (Fig. 3A), changing the inhibitory synapse location from 50 μm to 400 μm decreased the spine $[Ca^{2+}]_i$ only during the post-10-pre pairing (Fig. 3C–D) and suppressed tLTD (Fig. 3G). When the peak ΔW of the STDP curve was plotted as a function of IN synapse location from the soma, we found that the suppression of tLTD was greater for feedback inhibitory synapse more proximal to the CA3–CA1 synapse (Fig. 3I).

In the presence of a feedforward inhibitory synapse (Fig. 3B), changing the inhibitory synapse location from 50 μm to 400 μm decreased the spine $[Ca^{2+}]_i$ during both the pre-10-post and the post-10-pre pairing paradigms (Fig. 3E–F). The resulting STDP curve showed suppression of both tLTP and tLTD (Fig. 3H). When the peak ΔW of the STDP curve was plotted as a function of inhibitory synapse location from the soma, we found that feedforward inhibitory synapse proximal to the CA3–CA1 synapse suppressed both tLTP and tLTD more than distal synapses did (Fig. 3J). Also, feedforward inhibitory synapse location coinciding with CA3–CA1 synapse location could even completely block STDP. These results suggest that feedforward inhibitory synapse locations that are proximal to the CA3–CA1 synapse strongly modulate the STDP profile.

4. Discussion

Here, using a simple CA3–CA1 network model that consists of a presynaptic CA3 PC, a postsynaptic CA1 PC, and an IN, we demonstrated that feedforward and feedback inhibitory synaptic networks differentially influence the STDP profiles (Figs. 2 and 3). Feedback inhibitory networks that were activated by local recurrent inputs suppressed tLTD while mostly preserving tLTP (Figs. 2 and 3). In contrast, feedforward inhibitory networks that were activated by afferent inputs not only suppressed but also blocked both tLTP and tLTD (Fig. 3H–J), thus modulating both the strengthening and weakening of the CA3–CA1 synapse.

Single-spike pairings of pre- and postsynaptic neurons in our simple CA3–CA1 network model without inhibition reliably simulated the asymmetric STDP curve (Fig. 1E), as observed in cultured hippocampal neurons *in vitro* [2]. When feedforward or feedback inhibition was added to the CA3–CA1 network model, the overall asymmetric shape of the STDP curve was still maintained (Figs. 2 and 3G–H). Our result is in line with a previous computational modeling study where single GABAergic input that was simulated at different time points during the pre- and postsynaptic pairing of excitatory neurons preserved the asymmetric profile of the STDP curve [11].

The developmental block of tLTP induction with single-spike pairings in *in vitro* STDP experiments [6,7] was due to the maturation of $GABA_A$ receptor-mediated inhibition. However, the exact source of the inhibition is not yet known. In our simulation, somatic and proximal feedforward inhibitions onto CA1 PCs were most effective in suppressing tLTP, and it could even block tLTP induction (Fig. 3H and G). Single postsynaptic CA1 spike is sufficient in recruiting perisomatic feedforward inhibition to CA1 PCs [14,15,37], and feedforward inhibition is stronger in the somatic regions than in the dendrites [14]. Thus, the developmental block of tLTP induction might be due to the increased recruitment of

feedforward inhibition in the perisomatic and proximal dendritic regions provided by basket cells and bistratified cells, respectively [34,35]. Such feedforward inhibition could block the bAP [8] and block tLTP induction at the CA3–CA1 synapse. Interestingly, postsynaptic depolarization and increases in postsynaptic spike rates over 4 Hz have been shown to rescue the developmental block of tLTP with single-spike pairings at the mature hippocampal CA3–CA1 synapse [7]. An increased rate of postsynaptic spikes can switch from recruiting basket and bistratified cells that target proximal dendrites, to recruiting feedback oriens lacunosum-moleculare INs that target the distal dendrites in the stratum lacunosum-moleculare [13,15,17]. Our simulation results showed that distal feedback inhibition had minimal effects on tLTP induction (Fig. 3G). Therefore, the switch in spatial inhibitory networks by postsynaptic CA1 PC activity could have contributed to the rescue of tLTP by increasing postsynaptic spike frequencies in mature hippocampal slices. These results suggest that proximal feedforward inhibition could enhance signal [38] and coincidence detection [15] to directly influence STDP induction, whereas distal feedback inhibition might be more important for the integration of excitatory inputs, such as inputs from the entorhinal cortex [39] into distal dendrites of CA1 PC [15].

Here, we only investigated the STDP at the CA3–CA1 synapse between the CA3 PC and the CA1 PC. However, interneuronal synaptic plasticity also exists between INs and PCs [40,41]. Such interneuronal synaptic plasticity could regulate CA1 PC spiking and synaptic integration [42] to influence the STDP profile at the CA3–CA1 synapse. Thus, in the future, it will be important to incorporate interneuronal synaptic plasticity in order to develop a more physiologically realistic learning model of hippocampal networks.

In summary, we showed that $GABA_A$ receptor-mediated inhibition and its synaptic network structure can differentially modulate the STDP profile. GABAergic inhibitory networks change throughout life. For example, inhibition strengthens with development [45] and learning [43], while it weakens with the aging process, resulting in memory deficits [44]. Therefore, our results provide a computational evidence that inhibitory network is heavily involved in the spike timing-based hippocampal synaptic storage of memory.

Acknowledgments

This work was supported by the Basic Science Research Program (2012-0003500) and by the World Class University (WCU) program (R31-10008) through the National Research Foundation of Korea, funded by the Ministry of Education, Science, and Technology.

References

[1] S.J. Martin, P.D. Grimwood, R.G. Morris, Synaptic plasticity and memory: an evaluation of the hypothesis, Annu. Rev. Neurosci. 23 (2000) 649–711.
[2] G.Q. Bi, M.M. Poo, Synaptic modifications in cultured hippocampal neurons. dependence on spike timing synaptic strength and postsynaptic cell type, J. Neurosci. 18 (1998) 10464–10472.
[3] N. Caporale, Y. Dan, Spike timing-dependent plasticity: a Hebbian learning rule, Annu. Rev. Neurosci. 31 (2008) 25–46.
[4] T.F. Freund, G. Buzsaki, Interneurons of the hippocampus, Hippocampus 6 (1996) 347–470.
[5] J. Kwag, O. Paulsen, The timing of external input controls the sign of plasticity at local synapses, Nat. Neurosci. 12 (2009) 1219–1221.
[6] R.M. Meredith, A.M. Floyer-Lea, O. Paulsen, Maturation of long-term potentiation induction rules in rodent hippocampus role of GABAergic inhibition, J. Neurosci. 23 (2003) 11142–11146.
[7] J. Kwag, O. Paulsen, Gating of NMDA receptor-mediated hippocampal spike timing-dependent potentiation by mGluR5, Neuropharmacology 63 (2012) 701–709.
[8] H. Tsubokawa, W.N. Ross, IPSPs modulate spike backpropagation and associated [Ca2+]i changes in the dendrites of hippocampal CA1 pyramidal neurons, J. Neurophysiol. 76 (1996) 2896–2906.
[9] M. Nishiyama, K. Togashi, T. Aihara, K. Hong, GABAergic activities control spike timing- and frequency-dependent long-term depression at hippocampal excitatory synapses, Front. Synaptic Neurosci. 2 (2010) 22.
[10] S. Kubota, J. Rubin, T. Kitajima, Modulation of LTP/LTD balance in STDP by an activity-dependent feedback mechanism, Neural Network 22 (2009) 527–535.
[11] V. Cutsuridis, GABA inhibition modulates NMDA-R mediated spike timing dependent plasticity (STDP) in a biophysical model, Neural Network 24 (2011) 29–42.
[12] J.C. Lacaille, A.L. Mueller, D.D. Kunkel, P.A. Schwartzkroin, Local circuit interactions between oriens/alveus interneurons and CA1 pyramidal cells in hippocampal slices: electrophysiology and morphology, J. Neurosci. 7 (1987) 1979–1993.
[13] J.G. Pelletier, J.C. Lacaille, Long-term synaptic plasticity in hippocampal feedback inhibitory networks, Prog. Brain Res. 169 (2008) 241–250.
[14] F. Pouille, M. Scanziani, Enforcement of temporal fidelity in pyramidal cells by somatic feed-forward inhibition, Science 293 (2001) 1159–1163.
[15] F. Pouille, M. Scanziani, Routing of spike series by dynamic circuits in the hippocampus, Nature 429 (2004) 717–723.
[16] S. Karnup, A. Stelzer, Temporal overlap of excitatory and inhibitory afferent input in guinea-pig CA1 pyramidal cells, J. Physiol. 516 (Pt 2) (1999) 485–504.
[17] M. Bartos, H. Alle, I. Vida, Role of microcircuit structure and input integration in hippocampal interneuron recruitment and plasticity, Neuropharmacology 60 (2011) 730–739.
[18] M.L. Hines, N.T. Carnevale, The neuron simulation environment, Neural Comput. 9 (1997) 1179–1209.
[19] V. Cutsuridis, S. Cobb, B.P. Graham, Encoding and retrieval in a model of the hippocampal CA1 microcircuit, Hippocampus 20 (2010) 423–446.
[20] M. Migliore, D.A. Hoffman, J.C. Magee, D. Johnston, Role of an A-type K+ conductance in the back-propagation of action potentials in the dendrites of hippocampal pyramidal neurons, J. Comput. Neurosci. 7 (1999) 5–15.
[21] M. Migliore, L. Messineo, M. Ferrante, Dendritic Ih selectively blocks temporal summation of unsynchronized distal inputs in CA1 pyramidal neurons, J. Comput. Neurosci. 16 (2004) 5–13.
[22] C. Koch, Biophysics of Computation: Information Processing in Single Neurons, Oxford University Press, New York, 1999.
[23] N.A. Otmakhova, N. Otmakhov, J.E. Lisman, Pathway-specific properties of AMPA and NMDA-mediated transmission in CA1 hippocampal pyramidal cells, J. Neurosci. 22 (2002) 1199–1207.
[24] R.J. Sayer, M.J. Friedlander, S.J. Redman, The time course and amplitude of EPSPs evoked at synapses between pairs of CA3/CA1 neurons in the hippocampal slice, J. Neurosci. 10 (1990) 826–836.
[25] N. Spruston, P. Jonas, B. Sakmann, Dendritic glutamate receptor channels in rat hippocampal CA3 and CA1 pyramidal neurons, J. Physiol. 482 (Pt 2) (1995) 325–352.
[26] B.L. Sabatini, T.G. Oertner, K. Svoboda, The life cycle of Ca(2+) ions in dendritic spines, Neuron 33 (2002) 439–452.
[27] A.B. Ali, A.P. Bannister, A.M. Thomson, IPSPs elicited in CA1 pyramidal cells by putative basket cells in slices of adult rat hippocampus, Eur. J. Neurosci. 11 (1999) 1741–1753.
[28] E.H. Buhl, K. Halasy, P. Somogyi, Diverse sources of hippocampal unitary inhibitory postsynaptic potentials and the number of synaptic release sites, Nature 368 (1994) 823–828.
[29] E.H. Buhl, T. Szilagyi, K. Halasy, P. Somogyi, Physiological properties of anatomically identified basket and bistratified cells in the CA1 area of the rat hippocampus *in vitro*, Hippocampus 6 (1996) 294–305.
[30] D. Fricker, R. Miles, EPSP amplification and the precision of spike timing in hippocampal neurons, Neuron 28 (2000) 559–569.
[31] A.B. Ali, J. Deuchars, H. Pawelzik, A.M. Thomson, CA1 pyramidal to basket and bistratified cell EPSPs: dual intracellular recordings in rat hippocampal slices, J. Physiol. 507 (Pt 1) (1998) 201–217.
[32] J. Csicsvari, H. Hirase, A. Czurko, G. Buzsaki, Reliability and state dependence of pyramidal cell-interneuron synapses in the hippocampus: an ensemble approach in the behaving rat, Neuron 21 (1998) 179–189.
[33] J.E. Rubin, R.C. Gerkin, G.Q. Bi, C.C. Chow, Calcium time course as a signal for spike-timing-dependent plasticity, J. Neurophysiol. 93 (2005) 2600–2613.
[34] T. Klausberger, GABAergic interneurons targeting dendrites of pyramidal cells in the CA1 area of the hippocampus, Eur. J. Neurosci. 30 (2009) 947–957.
[35] T. Klausberger, P. Somogyi, Neuronal diversity and temporal dynamics: the unity of hippocampal circuit operations, Science 321 (2008) 53–57.
[36] P. Somogyi, T. Klausberger, Defined types of cortical interneurone structure space and spike timing in the hippocampus, J. Physiol. 562 (2005) 9–26.
[37] C.L. Torborg, T. Nakashiba, S. Tonegawa, C.J. McBain, Control of CA3 output by feedforward inhibition despite developmental changes in the excitation-inhibition balance, J. Neurosci. 30 (2010) 15628–15637.
[38] G. Buzsaki, Feed-forward inhibition in the hippocampal formation, Prog. Neurobiol. 22 (1984) 131–153.
[39] C.J. McBain, Multiple forms of feedback inhibition by str oriens inhibitory interneurons?, J Physiol. 524 (Pt 1) (2000) 2.
[40] K.P. Lamsa, J.H. Heeroma, P. Somogyi, D.A. Rusakov, D.M. Kullmann, Anti-Hebbian long-term potentiation in the hippocampal feedback inhibitory circuit, Science 315 (2007) 1262–1266.
[41] K. Lamsa, J.H. Heeroma, D.M. Kullmann, Hebbian LTP in feed-forward inhibitory interneurons and the temporal fidelity of input discrimination, Nat. Neurosci. 8 (2005) 916–924.

[42] F. Saraga, T. Balena, T. Wolansky, C.T. Dickson, M.A. Woodin, Inhibitory synaptic plasticity regulates pyramidal neuron spiking in the rodent hippocampus, Neuroscience 155 (2008) 64–75.
[43] S. Ruediger, C. Vittori, E. Bednarek, C. Genoud, P. Strata, B. Sacchetti, P. Caroni, Learning-related feedforward inhibitory connectivity growth required for memory precision, Nature 473 (2011) 514–518.
[44] E.M. Stanley, J.R. Fadel, D.D. Mott, Interneuron loss reduces dendritic inhibition and GABA release in hippocampus of aged rats, Neurobiol. Aging 33 (2012) 413–431.
[45] M.I. Banks, J.B. Hardie, R.A. Pearce, Development of GABA(A) receptor-mediated inhibitory postsynaptic currents in hippocampus, J. Neurophysiol. 88 (2002) 3097–3107.